

Gate-Voltage-Driven Quantum Phase Transition at $0.7(2e^2/h)$ in Quantum Point Contacts

Jongbae Hong

Asia Pacific Center for Theoretical Physics, Pohang, Gyeongbuk 37673, Korea

(Dated: February 27, 2025)

The complex gate-voltage-dependent differential conductance in quantum point contacts, shaped by entangled-state tunneling, was demonstrated through the movement of a localized spin. This spin responds to variations in side gate voltage, triggering a quantum phase transition (QPT) between symmetric and asymmetric Kondo coupling states, with the states separated by conductance regions $G \geq 0.7G_0$ and $G \leq 0.7G_0$, where $G_0 = 2e^2/h$, respectively. The asymmetric state has two Kondo temperatures, while the symmetric state has only one. The presence of two Kondo temperatures in the asymmetric state clarifies previously unresolved issues, such as the indeterminate Kondo temperature and anomalous behavior in the width of the zero-bias anomaly (ZBA) in the $G \leq 0.7G_0$ region. The QPT was investigated by analyzing the gate-voltage-dependent ZBA energy, calculated using the corresponding local density of states at the site of the localized spin, obtained during the replication of the differential conductance.

I. INTRODUCTION

The Kondo effect in nanoscale systems was first observed in quantum dots [1, 2], followed by quantum point contacts (QPCs) [3]. Kondo temperatures were determined through scaling analysis [1, 3]. Successful results support Kondo physics in both devices. However, puzzling features remain: below $0.7G_0$ in conductance, where $G_0 = 2e^2/h$ with electron charge e and Planck constant h , in QPCs, the scaling analysis fails, preventing the determination of the Kondo temperature [3]. The objective of this study is to answer the questions: Why is $0.7G_0$ special in the QPC and what happens to the QPC when the side gate voltage V_G passes the value giving conductance $0.7G_0$? These questions are difficult to answer because they ask about the fundamental dynamical aspects of the QPC since the conductance corresponds to the zero bias peak value of differential conductance, dI/dV vs. V , where I and V denote the source-drain current and applied bias, respectively, which carries the system dynamics.

A QPC exists in an entangled state that links the left and right electron reservoirs through a linearly combined two Kondo singlets formed by a spontaneously created localized spin in the narrow constriction of the QPC, as depicted in Fig. 1(a). The fundamental quantity carrying the dynamical information of the system is the local density of states (LDOS), $\rho_{d\sigma}(\omega)$, where d and σ denote the localized level and spin, respectively, as depicted in Fig. 1(a). With the LDOS, one may reveal the veiled properties of QPCs and answer the above questions. However, obtaining the LDOS amounts to solving the challenging non-equilibrium Kondo problem. Even worse is to treat complex V_G dependences [3–5].

Fortunately, the V_G dependence in a QPC has been studied using spin-density-functional theory calculations [6]. According to Ref. [6], the movement of the localized spin in the QPC is described as follows: initially created at a constriction edge at a low V_G , the localized spin migrates towards the center as V_G increases;

once it has reached the center, it remains there despite further increments in V_G . This process involves spontaneous symmetry breaking in the left–right Kondo coupling strength as V_G transitions from a higher ($V_G > V_G^c$) to a lower ($V_G < V_G^c$) value, where V_G^c denotes the point of symmetry breaking, as illustrated in Fig. 1(b). Such spontaneous symmetry breaking provides a sufficient condition for a continuous phase transition. Therefore, we aim to elucidate the existence of a V_G -driven quantum phase transition at V_G^c , corresponding to $0.7G_0$ in conductance, and to resolve the QPC puzzle.

Although spin-density-functional theory calculations produce two symmetric localized spins under equilibrium conditions [6, 7], a single localized spin effectively captures the electron dynamics under steady-state non-equilibrium conditions, as depicted in Fig. 1, which

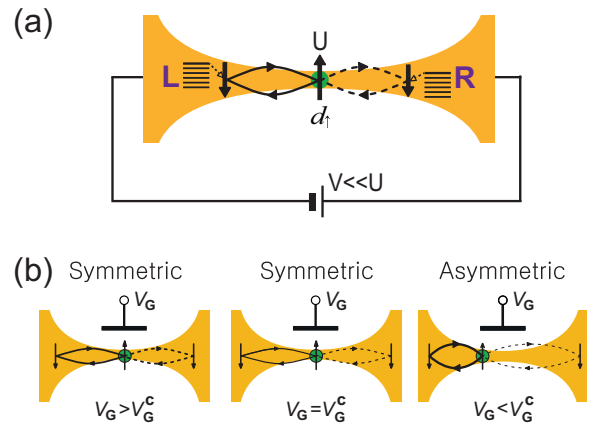


FIG. 1. (a) Schematic of the entangled-state tunneling via a linearly combined two Kondo singlets in QPCs. The downward arrows on both sides represent the coherent spins at the Fermi levels of the reservoirs. (b) Variation in the position of the localized spin and Kondo coupling strength (indicated by line thickness) due to the V_G . V_G^c denotes the point at which the symmetry breaks.

at equilibrium is described by the V_G -dependent two-reservoir Anderson impurity model,

$$\mathbf{H} = \sum_{\nu \in L, R} \sum_{\sigma, k} [\epsilon_k^\nu c_{k\sigma}^\nu c_{k\sigma}^\nu + \tilde{V}^\nu(V_G)(d_\sigma^\dagger c_{k\sigma}^\nu + c_{k\sigma}^\nu d_\sigma)] + \sum_{\sigma} \epsilon_d(V_G) d_\sigma^\dagger d_\sigma + U n_{d\uparrow} n_{d\downarrow}, \quad (1)$$

where $c_{k\sigma}^\nu$ ($c_{k\sigma}^{\nu\dagger}$), ϵ_k , $n_{d\uparrow}$, U , $\tilde{V}^\nu(V_G)$, and $\epsilon_d(V_G)$ represent, respectively, the annihilation (creation) operator of an electron with spin σ in quantum state k in reservoir ν , the electron kinetic energy of momentum k , the up-spin number operator $n_{d\uparrow} = d_\uparrow^\dagger d_\uparrow$, the Coulomb interaction at the site of the localized spin, the V_G -dependent hybridization strength, which is taken to be real and k -independent for simplicity, and the V_G -dependent energy of the localized d level. When the source-drain bias is lower than U , the coherent electrons in both reservoirs form an entangled state, and perform a unidirectional entangled-state tunneling, encompassing the dynamics of singlet co-tunneling and spin exchange.

The paper is organized as follows: In Sec. II, we present the V_G -dependent differential conductance formula, applicable to realistic conditions. We then introduce the Green's function technique in Liouville space, where basis vectors are operators, to derive a more tractable form of the differential conductance. In Sec. III, we reproduce experimental V_G -dependent differential conductance line shapes using this simplified formulation. Finally, in Sec. IV, we reveal a quantum phase transition by analyzing the V_G -dependent quasiparticle energy associated with the zero-bias anomaly (ZBA) peak. The paper concludes with a summary in Sec. V.

II. DIFFERENTIAL CONDUCTANCE

Our approach for determining the LDOS is based on experimentally measured differential conductance, which provides the only dynamic data available for phenomenological analysis. Therefore, a practical form of differential conductance is needed instead of the idealistic one, based on Meir–Wingreen current formula [8], and a manageable Green's function technique [9, 10], which yields a manageable form of differential conductance, is necessary. We address these issues in this section.

A. Gate-voltage-dependent formula

The Meir–Wingreen current formula, applicable to a system with a single-level interaction site situated between two reservoirs at different chemical potentials (illustrated in Fig. 1(a)), is expressed as follows [8]:

$$I = -\frac{2e}{h} \sum_{\sigma} \int d\omega [f_L^\sigma(\omega) - f_R^\sigma(\omega)] \tilde{\Gamma}(\omega) \text{Im} \mathcal{G}_{dd\sigma}^{+\text{sn}}(\omega), \quad (2)$$

where $\tilde{\Gamma}(\omega) = \Gamma^L(\omega)\Gamma^R(\omega)/[\Gamma^L(\omega) + \Gamma^R(\omega)]$, and $\Gamma^{L(R)}(\omega)$ is the left (right) coupling function. Here, we explicitly insert the superscript ‘sn’, indicating steady-state non-equilibrium. Our system exhibits spin-down symmetry, such that $\mathcal{G}_{dd\uparrow}^+(\omega) = \mathcal{G}_{dd\downarrow}^+(\omega)$. Since $f_{L(R)}^\uparrow(\omega) + f_{L(R)}^\downarrow(\omega) = f_{L(R)}(\omega)$, the formula simplifies to:

$$I = -\frac{2e}{h} \int d\omega [f_L(\omega) - f_R(\omega)] \tilde{\Gamma}(\omega) \text{Im} \mathcal{G}_{dd\uparrow}^{+\text{sn}}(\omega).$$

In this study, we consider the V_G -dependent current with ω -independent $\tilde{\Gamma}$. Thus, the V_G -dependent differential conductance at zero temperature is expressed as:

$$\frac{dI}{dV} = \frac{2e^2}{h} \tilde{\Gamma}^{\text{sn}}(V_G) \text{Im} \mathcal{G}_{dd\uparrow}^{+\text{sn}}(\omega, V_G) \Big|_{\hbar\omega=eV}. \quad (3)$$

This formula serves as a practical adaptation of an idealized expression based on the Meir–Wingreen current formula, Eq. (2). It assumes $\mathcal{G}_{dd\uparrow}^{+\text{sn}}(\omega, V_G)$ remains independent of the applied bias V , which is valid for entangled-state tunneling between two non-interacting reservoirs under sufficiently low bias.

The relationship $0 \leq \tilde{\Gamma}^{\text{sn}}(V_G) \leq \Delta$ holds, where the maximum value $\Delta = (\Gamma^L + \Gamma^R)/4$ occurs for $\Gamma^L = \Gamma^R$, corresponding to a left-right symmetric Kondo coupling state. Ideally, $\tilde{\Gamma}^{\text{sn}}(V_G)$ undergoes a non-analytic change at the point where $\Gamma^L = \Gamma^R$. However, under realistic conditions, $\tilde{\Gamma}^{\text{sn}}(V_G)$ is expected to vary smoothly. Both $\tilde{\Gamma}^{\text{sn}}(V_G)$ and $\text{Im} \mathcal{G}_{dd\uparrow}^{+\text{sn}}(\omega, V_G)$ are determined during the phenomenological replication of the experimental V_G -dependent dI/dV profile.

B. Green's function technique

In obtaining the differential conductance, the on-site retarded Green's function $\mathcal{G}_{dd\uparrow}^{+\text{sn}}(\omega)$ is the central quantity of interest, and the LDOS is given by the imaginary part of the on-site retarded Green's function, i.e., $\rho_{d\uparrow}^{\text{sn}}(\omega) = -(1/\pi) \text{Im} \mathcal{G}_{dd\uparrow}^{+\text{sn}}(\omega)$. $\mathcal{G}_{dd\uparrow}^{+\text{sn}}(\omega)$ is given by the dd element of the Green's function matrix, i.e., $i\mathcal{G}_{dd\uparrow}^{+\text{sn}}(\omega) = [1/(z\mathbf{I} + i\mathbf{H})]_{dd}$ or $i\mathcal{G}_{dd\uparrow}^{+\text{sn}}(\omega) = [1/(z\mathbf{I} + i\mathbf{L})]_{dd}$ [11], where $z = -i\omega + 0^+$, \mathbf{I} denotes the identity operator, and \mathbf{L} the Liouville operator.

As the superscript ‘sn’ implies, the matrix elements of \mathbf{H} or \mathbf{L} are obtained at steady-state nonequilibrium. A complete set of basis vectors or operators is needed to obtain the Green's function. For this reason, we opt for the Liouville space, as it facilitates the determination of basis operators.

1. Determining basis operators

Determining the basis operators is the first and most challenging step in obtaining the Green's function. We

developed a systematic method for identifying a complete set of basis operators describing the dynamics of $d_\sigma(t)$ driven by the single-reservoir Anderson impurity model [9], and extended it to the two-reservoir Anderson impurity model [10]. By excluding complex and insignificant basis operators, the complete set is divided into three groups:

- I : $\{d_\uparrow, \delta n_{d\downarrow} d_\uparrow\}$,
- II : $\{(\mathbf{L}_h^n \delta j_{d\downarrow}^{\pm L}) d_\uparrow, (\mathbf{L}_h^n \delta j_{d\downarrow}^{\pm R}) d_\uparrow\}$, $n = 0, 1, \dots, \infty$,
- III : $\{c_{k\uparrow}^{\nu}, \delta n_{d\downarrow} c_{k\uparrow}^{\nu}, (\mathbf{L}_h^n \delta j_{d\downarrow}^{\pm \nu}) c_{k\uparrow}^{\nu}\}$, $n, k = 0, 1, \dots, \infty$.

Here, δ denotes the deviation from the average, $j_{d\downarrow}^{-\nu} = i\tilde{V}^\nu \sum_k (c_{k\downarrow}^{\nu\dagger} d_\downarrow - d_\downarrow^\dagger c_{k\downarrow}^\nu)$, and $j_{d\downarrow}^{+\nu} = \tilde{V}^\nu \sum_k (c_{k\downarrow}^{\nu\dagger} d_\downarrow + d_\downarrow^\dagger c_{k\downarrow}^\nu)$. For $n = 2$, for example, $\mathbf{L}_h^2 \mathcal{O} = [\mathbf{H}_h, [\mathbf{H}_h, \mathcal{O}]]$, with $\mathbf{H}_h = \sum_{\sigma,k} \sum_{\nu \in L,R} \tilde{V}^\nu (d_\sigma^\dagger c_{k\sigma}^\nu + c_{k\sigma}^{\nu\dagger} d_\sigma)$ in Eq. (1). To ensure orthogonality among the basis operators, we introduced δ , where $\delta \mathcal{O} = \mathcal{O} - \langle \mathcal{O} \rangle$.

Group I describes the mediating site (MS) with a single level d , where the localized spin resides. Group II captures hybridization processes, while Group III characterizes the reservoirs. Applying \mathbf{L}_h to $j_{d\downarrow}^{\pm \nu}$ generates second-order hybridization terms between the ν reservoir and the MS. However, the full Liouville space describes the dynamics with such granularity that it renders the Green's function technique impractical. To construct a manageable Liouville space where this technique remains effective, we exclude the following basis operators: $\delta n_{d\downarrow} d_\uparrow$ in Group I, which represents on-site Coulomb interactions, and $(\mathbf{L}_h^n \delta j_{d\downarrow}^{\pm \nu}) d_\uparrow$ ($n = 1, 2, \dots, \infty$) and $(\mathbf{L}_h^n \delta j_{d\downarrow}^{\pm \nu}) c_{k\uparrow}^\nu$ ($n = 0, 1, \dots, \infty$) in Groups II and III, respectively, which describe multiple hybridizations. We keep operators $\delta n_{d\downarrow} c_{k\uparrow}^\nu$ $k = 0, 1, \dots, \infty$, describing nonvanishing entanglement, in Group III. See Fig. 2. The validity of these exclusions is supported by the excellent fit of our theoretical line shapes, characterized by Lorentzian peaks, to the experimental results [4], which suggests that multiple hybridization processes play a negligible role in the formation of coherent current through entangled-state tunneling. Thus, the working Liouville space with inner product $(\hat{a}, \hat{b}) = \langle \{\hat{a}, \hat{b}^\dagger\} \rangle$, where \hat{b}^\dagger is the adjoint of operator \hat{b} , and the angular and curly brackets represent the expectation and anti-commutator, respectively, is spanned by three groups of orthonormal basis operators [10, 12]:

- (i) d_\uparrow , describing the localized spin;
- (ii) $d_\uparrow \delta j_{d\downarrow}^{\pm L,R} / \langle (\delta j_{d\downarrow}^{\pm L,R})^2 \rangle^{1/2}$, describing the four hybridization types illustrated in Fig. 1(a);
- (iii) $c_{k\uparrow}^{L,R}$ and $c_{k\uparrow}^{L,R} \delta n_{d\downarrow} / \langle (\delta n_{d\downarrow})^2 \rangle^{1/2}$ with $k = 0, \dots, \infty$, describing the reservoirs.

2. Liouville matrix

We now symmetrically arrange the basis operators, as shown at the top of Fig. 2, and calculate the matrix elements $(i\mathbf{L})_{ij} = -\langle \{i[\mathbf{H}, \hat{e}_i], \hat{e}_j^\dagger\} \rangle$, where \hat{e}_i represents the i^{th} basis operator, and the square bracket denotes the commutator. The structure of the Liouville matrix is illustrated in Fig. 2.

Notably, the region of nonvanishing entanglement (highlighted in orange) is formed by matrix elements created by the hybridization operators and $c_{k\uparrow}^\nu \delta n_{d\downarrow}$ operators, as well as matrix elements between hybridization operators themselves. In contrast, the matrix elements formed by hybridization and $c_{k\uparrow}^\nu$ operators yield vanishing entanglement (cyan). The explicit form of the matrix $\mathbf{M} := z\mathbf{I} + i\mathbf{L}$ is provided in Fig. 6 in Appendix A.

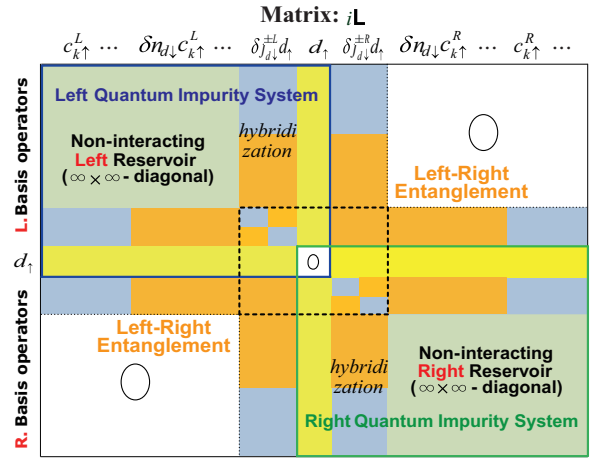


FIG. 2. Structure of the Liouville matrix: the reservoir (green), vanishing (cyan) and nonvanishing (orange) entanglements, and overlap between d_\uparrow and other basis operators (yellow).

3. Manageable form of differential conductance

The matrix reduction scheme [13, 14] detailed in Appendix A transforms the $\infty \times \infty$ matrix \mathbf{M} into an equivalent 5×5 matrix \mathbf{M}_r , which corresponds to tracing out the reservoir degrees of freedom. The resultant form of \mathbf{M}_r is given by [10, 12]

$$\mathbf{M}_r = \begin{pmatrix} -i\tilde{\omega} & \gamma^L & -U_{j-}^L & \gamma_S^{LR} & \gamma_A^{LR} \\ -\gamma^L & -i\tilde{\omega} & -U_{j+}^L & \gamma_A^{LR} & \gamma_S^{LR} \\ U_{j-}^{L*} & U_{j+}^{L*} & -i\tilde{\omega} & U_{j+}^{R*} & U_{j-}^{R*} \\ -\gamma_S^{LR} & -\gamma_A^{LR} & -U_{j+}^R & -i\tilde{\omega} & -\gamma^R \\ -\gamma_A^{LR} & -\gamma_S^{LR} & -U_{j-}^R & \gamma^R & -i\tilde{\omega} \end{pmatrix} + i\mathbf{\Sigma}, \quad (4)$$

where the first term is the central dashed block in Fig. 2, while the second term, $i\mathbf{\Sigma}$, consists of elements given by $i\Sigma_{pq} = \eta_{pq}[i\Sigma_0^L(\omega) + i\Sigma_0^R(\omega)]$ with

self-energy of the non-interacting Anderson model [15]. The coefficients η_{pq} are discussed below. To express the self-energy $i\Sigma_0^\nu(\omega)$, we adopt a wide semi-elliptic band, $\rho_0(\omega) = \rho_0\sqrt{1 - (\omega^2/D^2)}$, with a wide bandwidth $2D$. Then, $i\Sigma_0^\nu(\omega) = \Delta^\nu[\sqrt{1 - (\omega^2/D^2)} + i\omega/D]$, where $\Delta^\nu = \pi(\tilde{V}^\nu)^2\rho_0$, and the coupling function $\Gamma^\nu(\omega)$ is defined as twice the imaginary part of $\Sigma_0^\nu(\omega)$, i.e., $\Gamma^\nu(\omega) = 2\pi(\tilde{V}^\nu)^2\rho_0(\omega)$. Since the bandwidth $2D$ is sufficiently wide, we treat $\Gamma^\nu(\omega)$ as a constant, written as $\Gamma^\nu = 2\pi(\tilde{V}^\nu)^2\rho_0 = 2\Delta^\nu$. Each Δ^ν depends on V_G due to the V_G -dependent hybridization strength $\tilde{V}^\nu(V_G)$, though the sum $\Delta^L + \Delta^R$ remains constant. We use $\Delta = (\Delta^L + \Delta^R)/2$ as the energy unit in this study,

Meanwhile, the matrix elements of the first term of Eq. (4) are given by $\tilde{\omega} = \omega - \epsilon_d - U\langle n_{d\downarrow} \rangle$,

$$\gamma^{L(R)} = \frac{\langle \sum_k i(\tilde{V}^L c_{k\uparrow}^L + \tilde{V}^R c_{k\uparrow}^R) d_{\uparrow}^\dagger [j_{d\downarrow}^{-L(R)}, j_{d\downarrow}^{+L(R)}] \rangle^{\text{sn}}}{\langle (\delta j_{d\downarrow}^{-L(R)})^2 \rangle^{1/2} \langle (\delta j_{d\downarrow}^{+L(R)})^2 \rangle^{1/2}}, \quad (5)$$

$$\gamma_S^{LR} = \frac{\langle \sum_k i(\tilde{V}^L c_{k\uparrow}^L + \tilde{V}^R c_{k\uparrow}^R) d_{\uparrow}^\dagger [j_{d\downarrow}^{-L}, j_{d\downarrow}^{+R}] \rangle^{\text{sn}}}{\langle (\delta j_{d\downarrow}^{-L})^2 \rangle^{1/2} \langle (\delta j_{d\downarrow}^{+R})^2 \rangle^{1/2}}, \quad (6)$$

$$\gamma_A^{LR} = \frac{\langle \sum_k i(\tilde{V}^L c_{k\uparrow}^L + \tilde{V}^R c_{k\uparrow}^R) d_{\uparrow}^\dagger [j_{d\downarrow}^{-L}, j_{d\downarrow}^{-R}] \rangle^{\text{sn}}}{\langle (\delta j_{d\downarrow}^{-L})^2 \rangle^{1/2} \langle (\delta j_{d\downarrow}^{-R})^2 \rangle^{1/2}}, \quad (7)$$

and

$$U_{j^\mp}^\nu = i \frac{U \langle [n_{d\downarrow}, j_{d\downarrow}^{\mp\nu}] (1 - 2n_{d\uparrow}) + j_{d\downarrow}^{\mp\nu} (1 - 2\langle n_{d\downarrow} \rangle) \rangle^{\text{eq}}}{\langle (\delta j_{d\downarrow}^{\mp\nu})^2 \rangle^{1/2}}, \quad (8)$$

where the superscript ‘eq’ in $U_{j^\mp}^\nu$ indicates that the expectation is taken at equilibrium. The calculation procedures are detailed in Appendix B.

The elements $U_{j^\mp}^\nu$ represent the effective Coulomb interaction screened by the dynamics $j_{d\downarrow}^{-\nu}$ or $j_{d\downarrow}^{+\nu}$ coming from or directed towards the ν reservoir. Furthermore, the imaginary part of $U_{j^\mp}^\nu$, represented by the second term, vanishes at half-filling, as is the case in this study.

We finally arrive at a more manageable form of differential conductance:

$$\frac{dI}{dV} = \frac{2e^2}{h} \tilde{\Gamma}^{\text{sn}}(V_G) \text{Re}(\mathbf{M}_r^{-1})_{33} \Big|_{\hbar\tilde{\omega}=\epsilon V}. \quad (9)$$

III. REPLICATING dI/dV LINE SHAPES

Our first goal is to replicate the experimental differential conductance line shapes. Replicating the V_G -dependent differential conductance is achieved by phenomenologically determining the parameters involved in Eq. (9). The guidelines for determining these parameters are provided by atomic limit analysis

($\text{Im}\Sigma(\omega) \rightarrow 0$) [10, 12]. For a large on-site Coulomb interaction U at half-filling ($\text{Im}[U_{j^\pm}^{L,R}] = 0$), which is the case in this study, the atomic limit analysis provides the following insights:

- (a) The ZBA spectral weight is given by $8(\gamma^L\gamma^R)^2/[U^2\{(\gamma^L)^2 + (\gamma^R)^2\}]$;
- (b) The spectral weight of the coherent side peak is $8(\gamma_{S,A}^{LR}/U)^2$;
- (c) The positions of the two coherent side peaks are $\pm\sqrt{[(\gamma^L)^2 + (\gamma^R)^2]}/2$;
- (d) Coulomb peaks at $\pm U/2$ are produced with $U_{j^\pm}^{L,R} = U/4$ and $\gamma^{L,R} = \gamma_{S,A}^{LR} = 0$.

The equality $\gamma_S^{LR} = \gamma_A^{LR}$ is established under unidirectional entangled-state tunneling, as explained in the end of Appendix B 2. Using items (a)-(c), the values of γ^L and γ^R can be determined by the position of the side peak in the differential conductance, while $\gamma_{S,A}^{LR}$ are fixed by the spectral weight of the side peak, and $\gamma_{S,A}^{LR}$ play a crucial role in studying correlated superconductors, where only the side peak is present [16, 17]. Meanwhile, item (d) sets the non-entangled portion of η_{pq} to 0.25, except for η_{33} .

We set $U_{j^-}^L = U_{j^-}^R$ because the operator j^- indicates the steady current. We further observed that the matrix element $U_{j^+}^{L,R}$ adjusts the gap between the maxima of the ZBA and the side peak, while $U_{j^-}^{L,R}$ controls the distance between the minimum and maximum of the ZBA and side peak, respectively.

Given the asymmetry in the experimental dI/dV line shapes with respect to the applied bias, as reported in Ref. 4, we focused on fitting the central and right-

TABLE I. Variation of parameters with V_G

V_G	γ^L	γ^R	$\gamma_{S,A}^{LR}$	$U_{j^+}^L$	$U_{j^+}^R$	$U_{j^-}^{L,R}$	$\tilde{\Gamma}^{\text{sn}}$
17	0.64	0.64	0.64	0.4457	0.4457	0.323	1.012
16	0.62	0.62	0.62	0.4928	0.4928	0.385	1.003
15	0.59	0.59	0.59	0.5351	0.5351	0.435	0.995
14	0.56	0.56	0.56	0.5788	0.5788	0.488	0.980
13	0.535	0.535	0.56	0.6524	0.6524	0.560	0.962
12	0.510	0.510	0.55	0.7466	0.7466	0.647	0.937
11	0.495	0.495	0.565	0.8614	0.8614	0.753	0.904
10	0.484	0.484	0.595	1.0055	1.0055	0.897	0.856
9	0.495	0.495	0.68	1.2070	1.2070	1.0973	0.790
8	0.492	0.431	0.73	1.3963	1.1445	1.1445	0.697
7	0.488	0.409	0.84	1.7020	1.1946	1.1916	0.598
6	0.483	0.387	0.95	2.0935	1.3032	1.2388	0.508
5	0.477	0.314	1.04	2.5718	1.5688	1.2859	0.395
4	0.470	0.230	0.95	3.1193	1.8263	1.3331	0.296
3	0.462	0.210	0.95	3.6437	2.0703	1.3802	0.144

hand-side peaks. A semi-elliptic band with a width of 50Δ was employed, where the energy unit $\Delta = 1.083$ meV. The best fit was obtained using the parameters listed in Table 1 and the self-energy coefficients: $\eta_{11} = \eta_{15} = \eta_{55} = 0.253$, $\eta_{12} = \eta_{14} = \eta_{25} = \eta_{45} = 0.254$, $\eta_{22} = \eta_{24} = \eta_{44} = 0.260$, and $\eta_{33} = 1$ (exact) with symmetrical indices. The incremental deviation from $\eta_{pq} = 0.25$, attributed to left-right entanglement, is described by the relationships $\eta_{11} = \eta_{15} = \eta_{55} < \eta_{12} = \eta_{14} = \eta_{25} = \eta_{45} < \eta_{22} = \eta_{24} = \eta_{44}$. These relationships are thoroughly analyzed in Appendix C.

The theoretical results were superimposed on the experimental data from Ref. 4 in Fig. 3(a), with the corresponding LDOS shown in Fig. 3(b), thereby addressing our first goal and the most challenging aspects of this study. Notably, the peak value of the ZBA at $V_G = 9$ is $0.7(2e^2/h)$, signifying that $G = 0.7G_0$. By comparing Fig. 2(c) of Ref. 4 with the zero-bias peak values of Fig. 3(a), realistic values for $V_G = 3$ and $V_G = 9$ were found to be 0.067 V and 0.085 V, respectively, with each V_G step being 3.0 mV. The V_G -dependent behaviors of the γ 's, $\tilde{\Gamma}^{\text{sn}}(V_G)$, and $U_{j\pm}^{L,R}$ are shown in Fig. 3(c), its inset, and Fig. 3(d), respectively.

The trends of γ^L and γ^R shown in Fig. 3(c) clearly demonstrate the distinction between symmetric ($\gamma^L = \gamma^R$) and asymmetric ($\gamma^L \neq \gamma^R$) states at $V_G = 9$. We clarify in section IV that γ^L and γ^R differ by the Kondo coupling strengths on the left and right side of the localized spin, respectively.

The scaling puzzle in QPCs has been resolved by identifying the asymmetric Kondo coupling state with two distinct Kondo temperatures that occurs below $0.7G_0$. Since scaling analysis presupposes a single Kondo temperature for a given V_G , anomalies such as the indeterminate Kondo temperature and the anomalous behavior of the ZBA width below $0.7G_0$ arise when two Kondo temperatures coexist.

IV. QUANTUM PHASE TRANSITION

Identifying a quantum phase transition between symmetric and asymmetric Kondo coupling states, the central focus of this study, is both fundamental and interesting. To achieve this, we examine the quasiparticle energy at the Fermi level, specifically the ZBA energy, defined as:

$$E_{\text{ZBA}} = 2 \int_0^{\tilde{\omega}_{\min}} \tilde{\omega} \rho_{d\sigma}^{\text{sn}}(\tilde{\omega}) d\tilde{\omega}, \quad (10)$$

where $\tilde{\omega}_{\min}$ denotes the position of the local minimum in the LDOS shown in Fig. 3(b). Equation (10) provides a consistent method for estimating the ZBA energy. Using this approach, we determined the V_G -dependent ZBA energies at zero temperature and plotted them on a logarithmic scale against V_G in Fig. 4(a).

The data align remarkably well with two straight lines of different slopes, indicating a phase transition

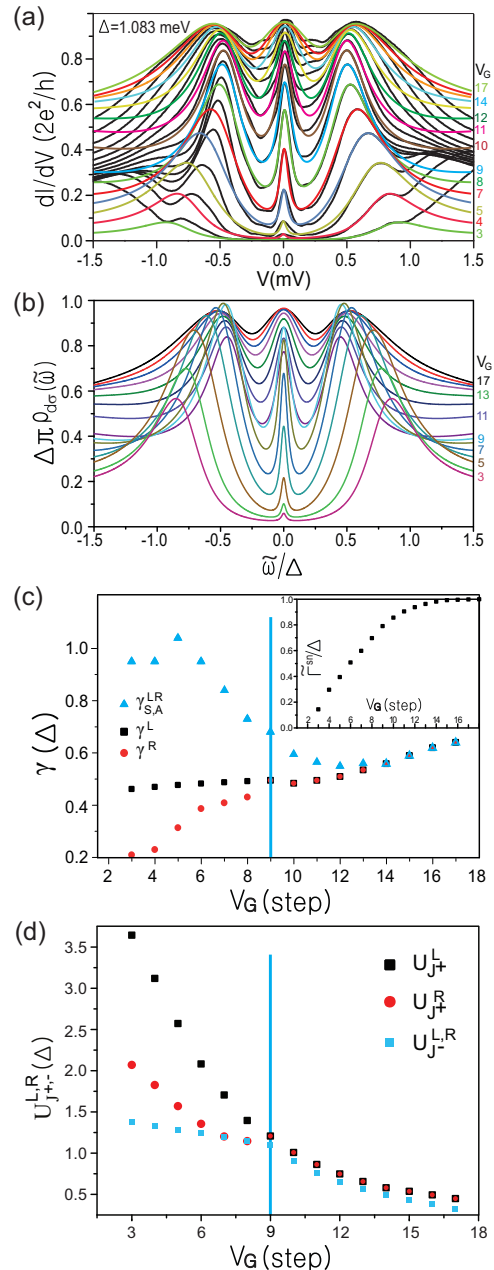


FIG. 3. (a) The colored curves superimposed on the experimental data (black) [4] represent the theoretical dI/dV line shapes. (b) The V_G -dependent local density of states. (c) The V_G -dependent behaviors of γ 's. The blue line indicates the point of $\gamma^L = \gamma^R$. Inset: $\tilde{\Gamma}^{\text{sn}}(V_G)$. (d) V_G -dependent behaviors of U_{j+}^L , U_{j+}^R , and $U_{j-}^{L,R}$. These are regarded real numbers in this study.

at $V_G = 9$ and suggesting distinct power-law behaviors: $E_{\text{ZBA}}/\Delta = 0.00671 - 0.00266 \times |V_G - 9|^{0.666}$ for $V_G \leq 9$ and $E_{\text{ZBA}}/\Delta = 0.00671 + 0.00200 \times |V_G - 9|^{1.169}$ for $V_G \geq 9$. As a result, the derivative $\partial E_{\text{ZBA}}/\partial V_G$ diverges as V_G approaches the critical point $V_G^c = 9$ from below, while it vanishes as V_G approaches the critical point from above, as shown in Fig. 4(b). This pronounced difference

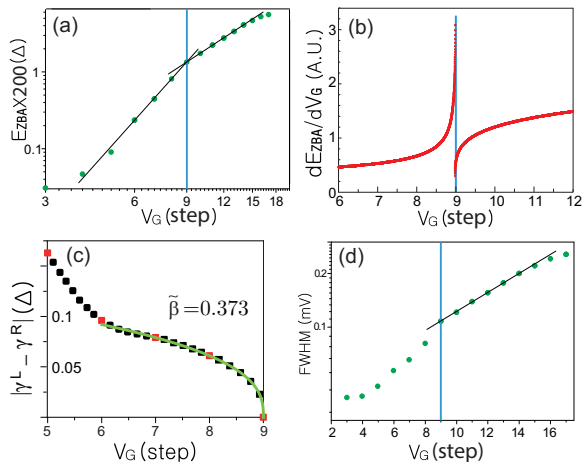


FIG. 4. (a) The behaviors of the ZBA energy on a logarithmic scale. (b) The derivative of the ZBA energy against V_G on a linear scale. (c) The critical behavior of the order parameter. The red squares represent the data, and the dark squares are provided for visual aid. (d) The ZBA width on a semilogarithmic scale.

at the transition point suggests the potential for developing quantum sensors.

Figures 4(a) and 4(b) confirm the presence of a continuous phase transition. In the context of such transitions, identifying an appropriate order parameter is crucial. We propose $|\gamma^L - \gamma^R|$ as the order parameter for this phase transition. The critical behavior is described by the relationship: $|\gamma^L - \gamma^R| \propto |V_G - V_G^c|^\beta$, where the critical exponent is determined to be $\tilde{\beta} = 0.373$, as illustrated in Fig. 4(c). The rationale for choosing $|\gamma^L - \gamma^R|$ as the order parameter is explained below.

Additionally, we explicitly illustrate the well-known single-Kondo-temperature behavior of the full width at half maximum (FWHM) of the ZBA peak, $\ln(\text{FWHM}) \propto |V_G - V_G^c|$, on a semilogarithmic scale in Fig. 4(d). Notably, the well-fitting region is confined to the symmetric Kondo coupling regime, $V_G \geq V_G^c$.

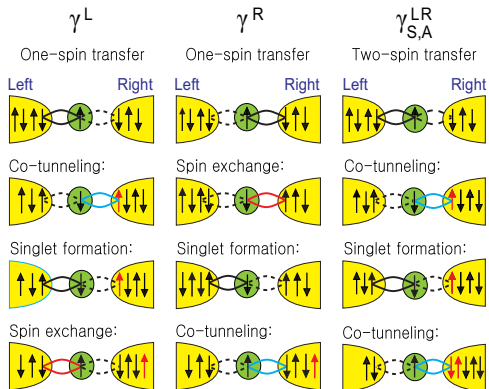


FIG. 5. Unidirectional entangled-state tunneling represented by the parameters γ 's.

To clarify the order parameter, it is necessary to elucidate the dynamics embedded within the matrix elements of \mathbf{M}_r . Meaningful dynamics representing the steady-state current is represented in the numerator of matrix element. We first consider $\gamma^{L(R)}$ given in Eq. (5).

To analyze the dynamics in the numerator, an expectation scheme tailored for a system under steady-state non-equilibrium conditions is essential. Unlike equilibrium systems, where the expectation scheme is universally defined, the non-equilibrium expectation must be established on a case-by-case basis. For the bias direction illustrated in Fig. 1(a), we define the non-equilibrium expectation as:

$$\langle 6 \text{ operators} \rangle^{\text{sn}} := \langle \Psi_0 | c_{k\uparrow}^{R\dagger} (6 \text{ operators}) d_{\uparrow} | \Psi_0 \rangle, \quad (11)$$

where the operators d_{\uparrow} and $c_{k\uparrow}^{R\dagger}$ are added to represent the initial and final events of a cyclic steady-state process, respectively. The ground state $|\Psi_0\rangle = |\Psi_L\rangle|\Psi_R\rangle$ describes the combined electron configurations at the Fermi surface of the left (L) and right (R) reservoirs. This definition establishes the cyclic fourth-order hybridization dynamics necessary for characterizing the steady-state flow under non-equilibrium conditions.

In γ^L , for instance, the unidirectional entangled-state tunneling is formed by selecting the operators $\tilde{V}^L c_{k\uparrow}^L d_{\uparrow}^{\dagger}$ from $(\tilde{V}^L c_{k\uparrow}^L + \tilde{V}^R c_{k\uparrow}^R) d_{\uparrow}^{\dagger}$, $(\tilde{V}^L)^2 c_{k\downarrow}^L d_{\downarrow} d_{\downarrow}^{\dagger} c_{k\downarrow}^L$ from the commutator $[j_{d\downarrow}^{-L}, j_{d\downarrow}^{+L}]$, and $c_{k\uparrow}^{R\dagger} d_{\uparrow}$ from the definition given above. These selected operators are then rearranged as $(\tilde{V}^L)^3 (d_{\uparrow}^{\dagger} c_{k\downarrow}^L) (c_{k\uparrow}^L d_{\downarrow}) (c_{k\uparrow}^{R\dagger} d_{\downarrow}^{\dagger}) (c_{k\downarrow}^L d_{\uparrow})$, depicted in the left-most panel of Fig. 5, representing: (left singlet formation) \rightarrow (singlet co-tunneling) \rightarrow (singlet formation on the left) \rightarrow (spin exchange). Similarly, the tunneling dynamics of γ^R and $\gamma_{S,A}^{L,R}$ are presented in the central and rightmost panels of Fig. 5, respectively.

Dividing the numerators of γ 's by $\tilde{V}^{\nu} \tilde{V}^{\nu'}$ in the denominators gives the same hybridization strength \tilde{V}^L to all γ 's. Consequently, γ^L and γ^R do not differ by hybridization strength but by their positions of spin exchange with different Kondo coupling strength, as illustrated in Figs. 4 and 1(b). Thus, the difference $|\gamma^L - \gamma^R|$ serves as the order parameter of the phase transition.

V. CONCLUSION

We identified a gate-voltage-driven quantum phase transition at V_G^c , where $G = 0.7G_0$, based on the V_G -dependent behavior of localized spin [6]. This study reveals two distinct phases: one phase ($G \geq 0.7G_0$) with left-right symmetric Kondo couplings and a single Kondo temperature, and the other ($G \leq 0.7G_0$) with left-right asymmetric Kondo couplings and two Kondo temperatures. This insight addresses puzzling behaviors observed in quantum point contacts, such as the

indeterminate Kondo temperature, deviation of scaled data from the scaling function [3], and the anomalous V_G -dependent width of the ZBA [3–5] in the $G \leq 0.7G_0$ region.

ACKNOWLEDGMENTS

This research was supported by the Korea National Research Foundation grant 2021R1I1A1A01040722 and partially by the Open KIAS center, KIAS, Korea.

Appendix A: Matrix reduction

The matrix representation of the Laplace-transformed on-site retarded Green's function, $i\mathcal{G}_{dd\uparrow}^+(z) = \text{LT}\langle\{d_\uparrow(t), d_\uparrow^\dagger\}\rangle \equiv A_0(z)$, is expressed as: $\mathbf{M}\mathbf{A}_c = \mathbf{D}_c$, where $\mathbf{M} = z\mathbf{I} + i\mathbf{L}$, and \mathbf{A}_c and \mathbf{D}_c are column vectors, defined as $\mathbf{A}_c^T = (A_{\infty L}(z), \dots, A_{1L}(z), A_0(z), A_{1R}(z), \dots, A_{\infty R}(z))^T$ and $\mathbf{D}_c^T = (0, \dots, 0, 1, 0, \dots, 0)^T$, where the superscript T denotes the transpose. For example, $A_{jL}(z) = \text{LT}\langle\{\hat{e}_j^L(t), \hat{e}_j^{\dagger L}\}\rangle$, with the j -th basis operator from the left side, as depicted at the top of Fig. 5. For further details, refer to Ref. [9].

As shown in Fig. 6, the matrix \mathbf{M} consists of nine blocks: \mathbf{M}_{LL} ($\infty \times \infty$), \mathbf{M}_{Ld} ($5 \times \infty$), \mathbf{M}_{dL} ($\infty \times 5$), and \mathbf{M}_{dd} (5×5). The matrix equation is thus expressed as:

$$\begin{pmatrix} \mathbf{M}_{LL} & \mathbf{M}_{dL} & \mathbf{0} \\ \mathbf{M}_{Ld} & \mathbf{M}_{dd} & \mathbf{M}_{Rd} \\ \mathbf{0} & \mathbf{M}_{dR} & \mathbf{M}_{RR} \end{pmatrix} \begin{pmatrix} \mathbf{C}^L \\ \mathbf{C}^d \\ \mathbf{C}^R \end{pmatrix} = \begin{pmatrix} \mathbf{0} \\ \mathbf{I}_5 \\ \mathbf{0} \end{pmatrix}, \quad (\text{A1})$$

where $\mathbf{C}^L = (A_{\infty L}(z), \dots, A_{3L}(z))^T$, $\mathbf{C}^d =$

Basis Operators:		Matrix $\mathbf{M} : -i\omega\mathbf{I} + i\mathbf{L}$						
		$c_{k\uparrow}^L \dots$	$\delta n_{j\downarrow} c_{k\uparrow}^L \dots$	$\delta j_{1\downarrow}^L d_\uparrow, \delta j_{1\downarrow}^L d_\uparrow$	d_\uparrow	$\delta j_{1\downarrow}^R d_\uparrow, \delta j_{1\downarrow}^R d_\uparrow$	$\delta n_{j\downarrow} c_{k\uparrow}^R \dots$	$c_{k\uparrow}^R \dots$
$c_{k\uparrow}^L$	$\begin{pmatrix} i(\omega-\epsilon) & 0 & 0 \\ 0 & \ddots & 0 \\ 0 & 0 & -i(\omega-\epsilon) \end{pmatrix}$	$\mathbf{0}$	$\mathbf{0}$	$\mathbf{0}$	$\begin{pmatrix} i\tilde{V}^L \\ \vdots \\ i\tilde{V}^L \end{pmatrix}$	$\mathbf{0}$	$\mathbf{0}$	$\mathbf{0}$
$\delta n_{j\downarrow} c_{k\uparrow}^L$	$\mathbf{0}$	$\begin{pmatrix} -i(\omega-\epsilon) & 0 & 0 \\ 0 & \ddots & 0 \\ 0 & 0 & -i(\omega-\epsilon) \end{pmatrix}$	$\begin{pmatrix} \tilde{V}_{\sigma\downarrow}^L & \tilde{V}_{\sigma\downarrow}^L \\ \vdots & \vdots \\ \tilde{V}_{\sigma\downarrow}^L & \tilde{V}_{\sigma\downarrow}^L \end{pmatrix}$	$\mathbf{0}$	$\begin{pmatrix} \tilde{V}_{\sigma\downarrow}^L & \tilde{V}_{\sigma\downarrow}^L \\ \vdots & \vdots \\ \tilde{V}_{\sigma\downarrow}^L & \tilde{V}_{\sigma\downarrow}^L \end{pmatrix}$	$\mathbf{0}$	$\mathbf{0}$	Left-Right Entanglement
$\delta j_{1\downarrow}^L d_\uparrow$	$\mathbf{0}$	$\begin{pmatrix} -\tilde{V}_{\sigma\downarrow}^L \dots -\tilde{V}_{\sigma\downarrow}^L \\ \vdots \\ -\tilde{V}_{\sigma\downarrow}^L \dots -\tilde{V}_{\sigma\downarrow}^L \end{pmatrix}$	$\begin{pmatrix} -i\tilde{\omega} & \gamma^L & -U_\uparrow^L \\ \vdots & \vdots & \vdots \\ -\gamma^L & i\tilde{\omega} & -U_\uparrow^L \end{pmatrix}$	$\begin{pmatrix} \gamma^L & \gamma^L \\ \vdots & \vdots \\ \gamma^L & \gamma^L \end{pmatrix}$	$\begin{pmatrix} \gamma^L & \gamma^L \\ \vdots & \vdots \\ \gamma^L & \gamma^L \end{pmatrix}$	$\begin{pmatrix} -\tilde{V}_{\sigma\downarrow}^L \dots -\tilde{V}_{\sigma\downarrow}^L \\ \vdots \\ -\tilde{V}_{\sigma\downarrow}^L \dots -\tilde{V}_{\sigma\downarrow}^L \end{pmatrix}$	$\mathbf{0}$	$\mathbf{0}$
$\delta j_{1\downarrow}^R d_\uparrow$	$\mathbf{0}$	$\begin{pmatrix} -\tilde{V}_{\sigma\downarrow}^R \dots -\tilde{V}_{\sigma\downarrow}^R \\ \vdots \\ -\tilde{V}_{\sigma\downarrow}^R \dots -\tilde{V}_{\sigma\downarrow}^R \end{pmatrix}$	$\begin{pmatrix} -\gamma^R & -\gamma^R & -U_\uparrow^R \\ \vdots & \vdots & \vdots \\ -\gamma^R & -\gamma^R & -U_\uparrow^R \end{pmatrix}$	$\begin{pmatrix} U_\uparrow^R & U_\uparrow^R \\ \vdots & \vdots \\ U_\uparrow^R & U_\uparrow^R \end{pmatrix}$	$\begin{pmatrix} -i\tilde{\omega} & -\gamma^R \\ \vdots & \vdots \\ -\gamma^R & -i\tilde{\omega} \end{pmatrix}$	$\begin{pmatrix} \gamma^R & \gamma^R \\ \vdots & \vdots \\ \gamma^R & \gamma^R \end{pmatrix}$	$\begin{pmatrix} -\tilde{V}_{\sigma\downarrow}^R \dots -\tilde{V}_{\sigma\downarrow}^R \\ \vdots \\ -\tilde{V}_{\sigma\downarrow}^R \dots -\tilde{V}_{\sigma\downarrow}^R \end{pmatrix}$	$\mathbf{0}$
d_\uparrow	$\begin{pmatrix} -i\tilde{V}^L \dots -i\tilde{V}^L \\ \vdots \\ -i\tilde{V}^L \dots -i\tilde{V}^L \end{pmatrix}$	$\mathbf{0}$	$\mathbf{0}$	$\begin{pmatrix} U_\uparrow^L & U_\uparrow^L \\ \vdots & \vdots \\ U_\uparrow^L & U_\uparrow^L \end{pmatrix}$	$\begin{pmatrix} -i\tilde{\omega} & -\gamma^L \\ \vdots & \vdots \\ -\gamma^L & -i\tilde{\omega} \end{pmatrix}$	$\begin{pmatrix} \gamma^L & \gamma^L \\ \vdots & \vdots \\ \gamma^L & \gamma^L \end{pmatrix}$	$\begin{pmatrix} -\tilde{V}_{\sigma\downarrow}^L \dots -\tilde{V}_{\sigma\downarrow}^L \\ \vdots \\ -\tilde{V}_{\sigma\downarrow}^L \dots -\tilde{V}_{\sigma\downarrow}^L \end{pmatrix}$	$(\infty \times 5)$
$\delta j_{1\downarrow}^L d_\uparrow$	$\mathbf{0}$	$\begin{pmatrix} -\tilde{V}_{\sigma\downarrow}^L \dots -\tilde{V}_{\sigma\downarrow}^L \\ \vdots \\ -\tilde{V}_{\sigma\downarrow}^L \dots -\tilde{V}_{\sigma\downarrow}^L \end{pmatrix}$	$\begin{pmatrix} -\gamma^L & -\gamma^L & -U_\uparrow^L \\ \vdots & \vdots & \vdots \\ -\gamma^L & -\gamma^L & -U_\uparrow^L \end{pmatrix}$	$\begin{pmatrix} U_\uparrow^L & U_\uparrow^L \\ \vdots & \vdots \\ U_\uparrow^L & U_\uparrow^L \end{pmatrix}$	$\begin{pmatrix} -i\tilde{\omega} & -\gamma^L \\ \vdots & \vdots \\ -\gamma^L & -i\tilde{\omega} \end{pmatrix}$	$\begin{pmatrix} \gamma^L & \gamma^L \\ \vdots & \vdots \\ \gamma^L & \gamma^L \end{pmatrix}$	$\begin{pmatrix} -\tilde{V}_{\sigma\downarrow}^L \dots -\tilde{V}_{\sigma\downarrow}^L \\ \vdots \\ -\tilde{V}_{\sigma\downarrow}^L \dots -\tilde{V}_{\sigma\downarrow}^L \end{pmatrix}$	$\mathbf{0}$
$\delta j_{1\downarrow}^R d_\uparrow$	$\mathbf{0}$	$\begin{pmatrix} -\tilde{V}_{\sigma\downarrow}^R \dots -\tilde{V}_{\sigma\downarrow}^R \\ \vdots \\ -\tilde{V}_{\sigma\downarrow}^R \dots -\tilde{V}_{\sigma\downarrow}^R \end{pmatrix}$	$\begin{pmatrix} -\gamma^R & -\gamma^R & -U_\uparrow^R \\ \vdots & \vdots & \vdots \\ -\gamma^R & -\gamma^R & -U_\uparrow^R \end{pmatrix}$	$\begin{pmatrix} U_\uparrow^R & U_\uparrow^R \\ \vdots & \vdots \\ U_\uparrow^R & U_\uparrow^R \end{pmatrix}$	$\begin{pmatrix} -i\tilde{\omega} & -\gamma^R \\ \vdots & \vdots \\ -\gamma^R & -i\tilde{\omega} \end{pmatrix}$	$\begin{pmatrix} \gamma^R & \gamma^R \\ \vdots & \vdots \\ \gamma^R & \gamma^R \end{pmatrix}$	$\begin{pmatrix} -\tilde{V}_{\sigma\downarrow}^R \dots -\tilde{V}_{\sigma\downarrow}^R \\ \vdots \\ -\tilde{V}_{\sigma\downarrow}^R \dots -\tilde{V}_{\sigma\downarrow}^R \end{pmatrix}$	$\mathbf{0}$
$\delta n_{j\downarrow} c_{k\uparrow}^R$	$\mathbf{0}$	$\mathbf{0}$	$\begin{pmatrix} \tilde{V}_{\sigma\downarrow}^L & \tilde{V}_{\sigma\downarrow}^L \\ \vdots & \vdots \\ \tilde{V}_{\sigma\downarrow}^L & \tilde{V}_{\sigma\downarrow}^L \end{pmatrix}$	$\mathbf{0}$	$\begin{pmatrix} \tilde{V}_{\sigma\downarrow}^L & \tilde{V}_{\sigma\downarrow}^L \\ \vdots & \vdots \\ \tilde{V}_{\sigma\downarrow}^L & \tilde{V}_{\sigma\downarrow}^L \end{pmatrix}$	$\mathbf{0}$	$\mathbf{0}$	Left-Right Entanglement
$c_{k\uparrow}^R$	$\mathbf{0}$	$\mathbf{0}$	$\mathbf{0}$	$\mathbf{0}$	$\mathbf{0}$	$\mathbf{0}$	$\mathbf{0}$	$(\infty \times \infty)$

FIG. 6. The matrix elements of \mathbf{M} are explicitly displayed using the structure shown in Fig. 3 of the main text. The matrix \mathbf{M} consists of nine blocks, outlined by thin black lines, which are used during the matrix reduction process. The orange sectors indicate the left-right entanglement.

$(A_{2L}(z), A_{1L}(z), i\mathcal{G}_{dd\uparrow}^+(z), A_{1R}(z), A_{2R}(z))^T$, $\mathbf{C}^R = (A_{3R}(z), \dots, A_{\infty R}(z))^T$, $\mathbf{0}$ is an infinite-dimensional zero vector, and $\mathbf{I}_5 = (00100)^T$.

By eliminating \mathbf{C}^L and \mathbf{C}^R from the three independent equations coming from Eq. (A1), we derive a reduced matrix equation [13, 14]:

$$(\mathbf{M}_{dd} - \mathbf{M}_{Ld}\mathbf{M}_{LL}^{-1}\mathbf{M}_{dL} - \mathbf{M}_{Rd}\mathbf{M}_{RR}^{-1}\mathbf{M}_{dR})\mathbf{C}^d = \mathbf{I}_5. \quad (\text{A2})$$

Since \mathbf{M}_{LL} and \mathbf{M}_{RR} are diagonal matrices with elements $(-i\omega + 0^+) + i\epsilon_k$ ($k = 0, 1, \dots, \infty$), their inverses are straightforward to compute. Consequently, the latter two terms in parentheses in Eq. (A2) can be expressed as a 5×5 matrix with elements $i\Sigma_{pq} = \eta_{pq}[i\Sigma_0^L(\omega) + i\Sigma_0^R(\omega)]$, where $i\Sigma_0^L(\omega) = i\Sigma_{\mathbf{k}}(\tilde{V}^\nu)^2/(\omega - \epsilon_{\mathbf{k}} + i0^+) = \pi(\tilde{V}^\nu)^2\rho_0^\nu(\omega)$, and $\rho_0^\nu(\omega)$ denotes the density of states of the ν reservoir. The coefficients η_{pq} are detailed in Appendix C below. Thus, the equivalent 5×5 matrix equation becomes: $\mathbf{M}_r\mathbf{C}^d = \mathbf{I}_5$, where $\mathbf{M}_r = \mathbf{M}_{dd} + i\Sigma$. Substituting $\mathbf{C}^d = (A_{2L}(z), A_{1L}(z), i\mathcal{G}_{dd\uparrow}^+(z), A_{1R}(z), A_{2R}(z))^T$, the on-site retarded Green's function is given by:

$$i\mathcal{G}_{dd\uparrow}^+(\omega) = (\mathbf{M}_r^{-1})_{33} \equiv (\mathbf{M}_r^{-1})_{dd}. \quad (\text{A3})$$

The local density of states at the mediating site (MS), $\rho_{d\uparrow}(\omega)$, is then:

$$\rho_{d\uparrow}(\omega) = -\frac{1}{\pi}\text{Im}\mathcal{G}_{dd\uparrow}^+(\omega) = -\frac{1}{\pi}\text{Re}(\mathbf{M}_r^{-1})_{33}. \quad (\text{A4})$$

This expression is used to calculate the differential conductance as described in Eq. (9) in the main text.

Appendix B: Liouville matrix elements

To construct the Liouville matrix $i\mathbf{L}$ using the basis operators, we apply the inner product relationship: $(\hat{e}_i, \mathbf{L}\hat{e}_j) = -(\mathbf{L}\hat{e}_i, \hat{e}_j)$. The matrix element $(i\mathbf{L})_{ij}$ is thus given by: $(i\mathbf{L})_{ij} = (\hat{e}_i, i\mathbf{L}\hat{e}_j) = -\langle\{i[\mathbf{H}, \hat{e}_i], \hat{e}_j^\dagger\}\rangle$, according to the definition of the inner product, where \hat{e}_j denotes the j^{th} orthonormal basis operator. The angular, curly, and square brackets represent the expectation, anticommutator, and commutator, respectively.

Arranging the basis operators in symmetric order, as shown in Fig. 2 in the main text or Fig. 6 in Appendix A, gives the Liouville matrix $i\mathbf{L}$, composed of nine blocks:

$$i\mathbf{L} = \begin{pmatrix} i\mathbf{L}_{LL} & i\mathbf{L}_{dL} & \mathbf{0} \\ i\mathbf{L}_{Ld} & i\mathbf{L}_{dd} & i\mathbf{L}_{Rd} \\ \mathbf{0} & i\mathbf{L}_{dR} & i\mathbf{L}_{RR} \end{pmatrix}. \quad (\text{B1})$$

The block $i\mathbf{L}_{LL}$ ($i\mathbf{L}_{RR}$) is an $\infty \times \infty$ diagonal block, and the blocks $i\mathbf{L}_{dL}$ ($i\mathbf{L}_{dR}$) and $i\mathbf{L}_{Ld}$ ($i\mathbf{L}_{Rd}$) are $5 \times \infty$ and $\infty \times 5$ blocks, respectively, while the central block $i\mathbf{L}_{dd}$ is a 5×5 block. Moreover, they have the following properties: $i(\mathbf{L}_{dL}) = i(-\mathbf{L}_{Ld}^\dagger)$; $i(\mathbf{L}_{dR}) = i(-\mathbf{L}_{Rd}^\dagger)$; and the

block $i\mathbf{L}_{dR}$ ($i\mathbf{L}_{Rd}$) is point-symmetric with $i\mathbf{L}_{dL}$ ($i\mathbf{L}_{Ld}$) about the centre of $i\mathbf{L}$. On the other hand, all the blocks surrounding $i\mathbf{L}_{dd}$ are transformed into the self-energy via the matrix reduction procedure explained in Appendix C.

We now present detailed calculations of the matrix elements of $i\mathbf{L}$ explicitly for the single reservoir Anderson impurity model (SRAIM) for simplicity. The results for the two-reservoir Anderson impurity model (TRAIM) are provided without detailed procedure. The following operator identities are frequently used:

$$[\hat{A}\hat{B}, \hat{C}] = \hat{A}\{\hat{B}, \hat{C}\} - \{\hat{A}, \hat{C}\}\hat{B}, \quad (\text{B2})$$

$$\{\hat{A}, \hat{B}\hat{C}\} = \{\hat{A}, \hat{B}\}\hat{C} - \hat{B}\{\hat{A}, \hat{C}\} \quad \text{and} \quad (\text{B3})$$

$$\begin{aligned} \{\hat{A}\hat{B}, \hat{C}\hat{D}\} &= \hat{A}\{\hat{B}, \hat{C}\}\hat{D} + \{\hat{A}, \hat{C}\}\hat{B}\hat{D} + \hat{C}\{\hat{A}, \hat{D}\}\hat{B} \\ &\quad - \hat{C}\hat{A}\{\hat{B}, \hat{D}\}. \end{aligned} \quad (\text{B4})$$

1. Matrix elements of the block $i\mathbf{L}_{LL}$

The block $i\mathbf{L}_{LL}$ ($i\mathbf{L}_{RR}$) is composed of two infinite-dimensional diagonal blocks with elements $i\epsilon_k$ that are constructed by the basis operators $c_{k\uparrow}^\nu$ and $\delta n_{d\downarrow} c_{k\uparrow}^\nu$ with $k = 0, 1, \dots, \infty$ describing the ν reservoir. We skip the calculation procedure because it is simple.

2. Matrix elements of the block $i\mathbf{L}_{dd}$

The central block $i\mathbf{L}_{dd}$ is expressed as

$$i\mathbf{L}_{dd} = \begin{pmatrix} D_1 & \gamma^L & -U_{j^-}^L & \gamma_S^{LR} & \gamma_A^{LR} \\ -\gamma^L & D_2 & -U_{j^+}^L & \gamma_A^{LR} & \gamma_S^{LR} \\ U_{j^-}^{L*} & U_{j^+}^{L*} & D_3 & U_{j^+}^{R*} & U_{j^-}^{R*} \\ -\gamma_S^{LR} & -\gamma_A^{LR} & -U_{j^+}^R & D_4 & -\gamma^R \\ -\gamma_A^{LR} & -\gamma_S^{LR} & -U_{j^-}^R & \gamma^R & D_5 \end{pmatrix}. \quad (\text{B5})$$

We derive the expression of each matrix element through the calculations for the SRAIM.

a. Diagonal elements

The diagonal elements are given by $D_{1,2} = \langle \{i\mathbf{L}(\delta j_{d\downarrow}^\mp d_\uparrow), \delta j_{d\downarrow}^\mp d_\uparrow^\dagger\} \rangle$ and $D_3 = -\langle \{i\mathbf{L}d_\uparrow, d_\uparrow^\dagger\} \rangle$ for the SRAIM. Using the commutator $i[\mathbf{H}, d_\uparrow] = -i\sum_{\mathbf{k}} \tilde{V}c_{\mathbf{k}\uparrow} - i\epsilon_d d_\uparrow - iUd_\uparrow n_{d\downarrow}$ gives the diagonal elements as follows:

$$\begin{aligned} D_3 : \quad & - \langle \{i[\mathbf{H}, d_\uparrow], d_\uparrow^\dagger\} \rangle = i\sum_{\mathbf{k}} \tilde{V}\langle \{c_{\mathbf{k}\uparrow}, d_\uparrow^\dagger\} \rangle \\ & + i\epsilon_d \langle \{d_\uparrow, d_\uparrow^\dagger\} \rangle + iU\langle \{d_\uparrow n_{d\downarrow}, d_\uparrow^\dagger\} \rangle \\ & = i\epsilon_d + iU\langle \{d_\uparrow n_{d\downarrow}, d_\uparrow^\dagger\} \rangle = i\epsilon_d + iU\langle \{d_\uparrow, d_\uparrow^\dagger\} n_{d\downarrow} \rangle \\ & = i\epsilon_d + iU\langle n_{d\downarrow} \rangle, \end{aligned}$$

and

$$\begin{aligned} D_{1,2} : \quad & -\langle \{i[\mathbf{H}, d_\uparrow \delta j_{d\downarrow}^\mp], (d_\uparrow \delta j_{d\downarrow}^\mp)^\dagger\} \rangle \\ & = -\langle \{i[\mathbf{H}, d_\uparrow] \delta j_{d\downarrow}^\mp, \delta j_{d\downarrow}^\mp d_\uparrow^\dagger\} \rangle \\ & - \langle \{d_\uparrow i[\mathbf{H}, \delta j_{d\downarrow}^\mp], \delta j_{d\downarrow}^\mp d_\uparrow^\dagger\} \rangle. \end{aligned}$$

The first term of $D_{1,2}$ is rewritten as

$$\begin{aligned} & - \langle \{i[\mathbf{H}, d_\uparrow] \delta j_{d\downarrow}^\mp, \delta j_{d\downarrow}^\mp d_\uparrow^\dagger\} \rangle \\ & = \langle \{ (i\sum_{\mathbf{k}} \tilde{V}c_{\mathbf{k}\uparrow} + i\epsilon_d d_\uparrow + iUd_\uparrow n_{d\downarrow}) \delta j_{d\downarrow}^\mp, (d_\uparrow \delta j_{d\downarrow}^\mp)^\dagger \} \rangle \\ & = i\epsilon_d \langle \{d_\uparrow \delta j_{d\downarrow}^\mp, \delta j_{d\downarrow}^\mp d_\uparrow^\dagger\} \rangle + iU\langle \{d_\uparrow n_{d\downarrow} \delta j_{d\downarrow}^\mp, \delta j_{d\downarrow}^\mp d_\uparrow^\dagger\} \rangle. \end{aligned}$$

Applying the decoupling approximation, $n_{d\downarrow} \delta j_{d\downarrow}^\mp = \langle n_{d\downarrow} \rangle \delta j_{d\downarrow}^\mp$, to the U -term above gives rise to a form with squared norm:

$$-\langle \{i[\mathbf{H}, d_\uparrow] \delta j_{d\downarrow}^\mp, \delta j_{d\downarrow}^\mp d_\uparrow^\dagger\} \rangle = [i\epsilon_d + iU\langle n_{d\downarrow} \rangle] \times \|d_\uparrow \delta j_{d\downarrow}^\mp\|^2.$$

Meanwhile, the second term of $D_{1,2}$ vanishes using the relation $[\mathbf{H}, j_{d\downarrow}^\mp] \propto j_{d\downarrow}^\pm$ and the orthogonality condition of the basis operators. Thus, the diagonal elements of the block $i\mathbf{L}_{dd}$ for the SRAIM are $i\epsilon_d + iU\langle n_{d\downarrow} \rangle$.

b. Matrix elements $U_{j^\mp}^\nu$

The elements U_{j^\mp} for the SRAIM come from the inner product $-\langle \{i\mathbf{L}d_\uparrow, \delta j_{d\downarrow}^\mp d_\uparrow^\dagger\} \rangle$, i.e.,

$$\begin{aligned} & - \langle \{i[\mathbf{H}, d_\uparrow], \delta j_{d\downarrow}^\mp d_\uparrow^\dagger\} \rangle = i\epsilon_d \langle \delta j_{d\downarrow}^\mp \rangle \langle \{d_\uparrow, d_\uparrow^\dagger\} \rangle \\ & + iU\langle \{d_\uparrow n_{d\downarrow}, \delta j_{d\downarrow}^\mp d_\uparrow^\dagger\} \rangle + i\sum_{\mathbf{k}} \tilde{V}\langle \delta j_{d\downarrow}^\mp \rangle \langle \{c_{\mathbf{k}\uparrow}, d_\uparrow^\dagger\} \rangle \\ & = iU\langle \{d_\uparrow n_{d\downarrow}, \delta j_{d\downarrow}^\mp d_\uparrow^\dagger\} \rangle. \end{aligned}$$

Using the operator identity of Eq. (B4) yields

$$\begin{aligned} & \langle \{d_\uparrow \delta n_{d\downarrow}, \delta j_{d\downarrow}^\mp d_\uparrow^\dagger\} \rangle = \langle d_\uparrow d_\uparrow^\dagger [n_{d\downarrow}, j_{d\downarrow}^\mp] \rangle + \langle \delta j_{d\downarrow}^\mp \delta n_{d\downarrow} \rangle \\ & = \langle (1 - n_{d\uparrow}) [n_{d\downarrow}, j_{d\downarrow}^\mp] + \delta j_{d\downarrow}^\mp \delta n_{d\downarrow} \rangle \\ & = \langle (\frac{1}{2} - n_{d\uparrow}) [n_{d\downarrow}, j_{d\downarrow}^\mp] + \frac{1}{2} [\delta n_{d\downarrow}, \delta j_{d\downarrow}^\mp] + \delta j_{d\downarrow}^\mp \delta n_{d\downarrow} \rangle \\ & = \frac{1}{2} \langle (1 - 2n_{d\uparrow}) [n_{d\downarrow}, j_{d\downarrow}^\mp] + \{ \delta n_{d\downarrow}, \delta j_{d\downarrow}^\mp \} \rangle \\ & = \frac{1}{2} \langle \{ (1 - 2n_{d\uparrow}) [n_{d\downarrow}, j_{d\downarrow}^\mp] + (1 - 2\langle n_{d\downarrow} \rangle) \langle j_{d\downarrow}^\mp \rangle \} \rangle. \end{aligned}$$

Hence, the matrix elements $U_{j^\mp}^\nu$ for the TRAIM is given by

$$U_{j^\mp}^\nu = \frac{U}{2} \left[\frac{\langle i(1 - 2n_{d\uparrow}) [n_{d\downarrow}, j_{d\downarrow}^{\mp\nu}] \rangle + i(1 - 2\langle n_{d\downarrow} \rangle) \langle j_{d\downarrow}^{\mp\nu} \rangle}{\langle (\delta j_{d\downarrow}^{\mp\nu})^2 \rangle^{1/2}} \right]. \quad (\text{B6})$$

Note that the second term is the imaginary part, reflecting the departure from half-filling.

c. Matrix elements $\gamma^{L,R}$, $\gamma_S^{L,R}$, and $\gamma_A^{L,R}$

Matrix element γ for the SRAIM is given by

$$\begin{aligned} & - \langle \{i\mathbf{L}(d_\uparrow \delta j_{d\downarrow}^\mp), \delta j_{d\downarrow}^\pm d_\uparrow^\dagger\} \rangle = - \langle \{i[\mathbf{H}, d_\uparrow] \delta j_{d\downarrow}^\mp, \delta j_{d\downarrow}^\pm d_\uparrow^\dagger\} \rangle \\ & - \langle \{d_\uparrow i[\mathbf{H}, j_{d\downarrow}^\mp], \delta j_{d\downarrow}^\pm d_\uparrow^\dagger\} \rangle. \end{aligned} \quad (\text{B7})$$

The second term vanishes because the inner product contains a single $\delta j_{d\downarrow}^\pm$, while the first term is rewritten as

$$\begin{aligned} & - \langle \{i[\mathbf{H}, d_\uparrow] \delta j_{d\downarrow}^\mp, \delta j_{d\downarrow}^\pm d_\uparrow^\dagger\} \rangle \\ & = i\epsilon_d \langle \{d_\uparrow \delta j_{d\downarrow}^\mp, \delta j_{d\downarrow}^\pm d_\uparrow^\dagger\} \rangle + iU \langle \{d_\uparrow n_{d\downarrow} \delta j_{d\downarrow}^\mp, \delta j_{d\downarrow}^\pm d_\uparrow^\dagger\} \rangle \\ & + i \sum_{\mathbf{k}} \tilde{V} \langle \{c_{k\uparrow} \delta j_{d\downarrow}^\mp, \delta j_{d\downarrow}^\pm d_\uparrow^\dagger\} \rangle. \end{aligned} \quad (\text{B8})$$

The first and second terms of Eq. (B8) vanish by applying the orthogonality condition of the basis operators, $\langle \{d_\uparrow \delta j_{d\downarrow}^\pm, \delta j_{d\downarrow}^\mp d_\uparrow^\dagger\} \rangle = 0$, and decoupling approximation ($n_{d\downarrow}$) to the second term. Meanwhile, the third term of Eq. (B8) is rewritten as

$$\begin{aligned} & i \sum_{\mathbf{k}} \tilde{V} \langle \{c_{k\uparrow} \delta j_{d\downarrow}^\mp, \delta j_{d\downarrow}^\pm d_\uparrow^\dagger\} \rangle \\ & = i \sum_{\mathbf{k}} \tilde{V} \langle \{ \delta j_{d\downarrow}^\mp \delta j_{d\downarrow}^\pm c_{k\uparrow} d_\uparrow^\dagger - \delta j_{d\downarrow}^\pm \delta j_{d\downarrow}^\mp c_{k\uparrow} d_\uparrow^\dagger \} \rangle \\ & = i \sum_{\mathbf{k}} \tilde{V} \langle [\delta j_{d\downarrow}^\mp, \delta j_{d\downarrow}^\pm] c_{k\uparrow} d_\uparrow^\dagger \rangle = i \sum_{\mathbf{k}} \tilde{V} \langle [j_{d\downarrow}^\mp, j_{d\downarrow}^\pm] c_{k\uparrow} d_\uparrow^\dagger \rangle. \end{aligned}$$

Finally, the matrix element γ for the SRAIM is expressed as

$$\gamma = \frac{-\langle \{i\mathbf{L}(d_\uparrow \delta j_{d\downarrow}^\mp), \delta j_{d\downarrow}^\pm d_\uparrow^\dagger\} \rangle}{\sqrt{\langle (\delta j_{d\downarrow}^\mp)^2 \rangle} \sqrt{\langle (\delta j_{d\downarrow}^\pm)^2 \rangle}} = \frac{i \sum_{\mathbf{k}} \tilde{V} \langle [j_{d\downarrow}^\mp, j_{d\downarrow}^\pm] c_{k\uparrow} d_\uparrow^\dagger \rangle}{\sqrt{\langle (\delta j_{d\downarrow}^\mp)^2 \rangle} \sqrt{\langle (\delta j_{d\downarrow}^\pm)^2 \rangle}}.$$

For the TRAIM, the changes, such as $\tilde{V} c_{k\uparrow} \rightarrow (\tilde{V}^L c_{k\uparrow}^L + \tilde{V}^R c_{k\uparrow}^R)$ and $j_{d\downarrow}^\mp \rightarrow j_{d\downarrow}^{\nu}$ for ν with $\nu \in L, R$ give the right expressions for γ^L and γ^R . In contrast, for $\gamma_{S,A}^{L,R}$, further considerations, such as combinations of superscripts (L, R) and ($+, -$) are required to have the expressions given below. Finally, γ 's are written as:

$$\begin{aligned} \gamma^\nu & = \langle \sum_{\mathbf{k}} i(\tilde{V}^L c_{k\uparrow}^L + \tilde{V}^R c_{k\uparrow}^R) d_\uparrow^\dagger [j_{d\downarrow}^{-\nu}, j_{d\downarrow}^{+\nu}] \rangle^{\text{sn}}, \\ \gamma_S^{LR} & = \langle \sum_{\mathbf{k}} i(\tilde{V}^L c_{k\uparrow}^L + \tilde{V}^R c_{k\uparrow}^R) d_\uparrow^\dagger [j_{d\downarrow}^{-L}, j_{d\downarrow}^{+R}] \rangle^{\text{sn}}, \quad (\text{B9}) \\ \gamma_A^{LR} & = \langle \sum_{\mathbf{k}} i(\tilde{V}^L c_{k\uparrow}^L + \tilde{V}^R c_{k\uparrow}^R) d_\uparrow^\dagger [j_{d\downarrow}^{\mp L}, j_{d\downarrow}^{\mp R}] \rangle^{\text{sn}}, \end{aligned}$$

where the normalization factor $[\langle (\delta j_{d\downarrow}^{\mp\nu})^2 \rangle \langle (\delta j_{d\downarrow}^{\pm\nu'})^2 \rangle]^{1/2}$ in corresponding denominator was not written explicitly.

In contrast, the commutator of $\gamma_{S,A}^{LR}$ is given by $[j_{d\downarrow}^{-L}, j_{d\downarrow}^{+R}] = i\tilde{V}^L \tilde{V}^R (c_{k\downarrow}^L d_\downarrow d_\downarrow^\dagger c_{k\downarrow}^R - d_\downarrow^\dagger c_{k\downarrow}^R c_{k\downarrow}^L d_\downarrow - d_\downarrow^\dagger c_{k\downarrow}^L c_{k\downarrow}^R d_\downarrow + c_{k\downarrow}^R d_\downarrow d_\downarrow^\dagger c_{k\downarrow}^L)$, in which the first and fourth terms provide a symmetric combination of the leftward

and rightward movements, while γ_A^{LR} with $[j_{d\downarrow}^{-L}, j_{d\downarrow}^{-R}]$ yields an antisymmetric combination ($c_{k\downarrow}^L d_\downarrow d_\downarrow^\dagger c_{k\downarrow}^R - c_{k\downarrow}^R d_\downarrow d_\downarrow^\dagger c_{k\downarrow}^L$). Remaining terms in the commutators do not form unidirectional entangled-state tunneling, as discussed in the main text using the expectation for the steady-state non-equilibrium given in Eq. (11) in the main text. Thus, under a bias, the unidirectional entangled-state tunneling gives the equality $\gamma_S^{LR} = \gamma_A^{LR}$.

3. Matrix elements of the block $i\mathbf{L}_{dL}$

The block $i\mathbf{L}_{dL}$, for example, is written as

$$i\mathbf{L}_{dL} = \begin{bmatrix} \mathbf{0} & \mathbf{0} & i\mathbf{C}_{kd}^L & \mathbf{0} & \mathbf{0} \\ i\mathbf{C}_{kj^-}^{LL} & i\mathbf{C}_{kj^+}^{LL} & \mathbf{0} & i\mathbf{C}_{kj^+}^{LR} & i\mathbf{C}_{kj^-}^{LR} \end{bmatrix}, \quad (\text{B10})$$

where $i\mathbf{C}_{kd}^L$, $i\mathbf{C}_{kj^\mp}^{LL}$, and $i\mathbf{C}_{kj^\mp}^{LR}$ are infinite-dimensional column vectors, as shown in Fig. 6. The elements of $i\mathbf{C}_{kd}^L$ and $i\mathbf{C}_{kj^\mp}^{LL}$ are given by $-\langle \{i\mathbf{L}c_{k\uparrow}, d_\uparrow^\dagger\} \rangle$ and $-\langle \{i\mathbf{L}(c_{k\uparrow} \delta n_{d\downarrow}), \delta j_{d\downarrow}^\mp d_\uparrow^\dagger\} \rangle$, respectively. Note that the calculations are done for the SRAIM. Thus, they are given as follows:

$$\begin{aligned} i\mathbf{C}_{kd} & = -\langle \{i\mathbf{L}c_{k\uparrow}, d_\uparrow^\dagger\} \rangle = -\langle \{i[\mathbf{H}, c_{k\uparrow}], d_\uparrow^\dagger\} \rangle \\ & = i\epsilon_k \langle \{c_{k\uparrow}, d_\uparrow^\dagger\} \rangle + i\tilde{V} \langle \{d_\uparrow, d_\uparrow^\dagger\} \rangle = i\tilde{V} \end{aligned} \quad (\text{B11})$$

and

$$\begin{aligned} i\mathbf{C}_{kj^\mp} & = -\langle \{i\mathbf{L}(c_{k\uparrow} \delta n_{d\downarrow}), \delta j_{d\downarrow}^\mp d_\uparrow^\dagger\} \rangle \\ & = -\langle \{i[\mathbf{H}, c_{k\uparrow} \delta n_{d\downarrow}], \delta j_{d\downarrow}^\mp d_\uparrow^\dagger\} \rangle \\ & = -\langle \{i[\mathbf{H}, c_{k\uparrow}] \delta n_{d\downarrow} + c_{k\uparrow} i[\mathbf{H}, n_{d\downarrow}], \delta j_{d\downarrow}^\mp d_\uparrow^\dagger\} \rangle \\ & = i\epsilon_k \langle \{c_{k\uparrow} \delta n_{d\downarrow}, \delta j_{d\downarrow}^\mp d_\uparrow^\dagger\} \rangle + i\tilde{V} \langle \{d_\uparrow \delta n_{d\downarrow}, \delta j_{d\downarrow}^\mp d_\uparrow^\dagger\} \rangle \\ & - \langle \{c_{k\uparrow} j_{d\downarrow}^-, \delta j_{d\downarrow}^\mp d_\uparrow^\dagger\} \rangle. \end{aligned} \quad (\text{B12})$$

The first term $i\epsilon_k \langle \{c_{k\uparrow} \delta n_{d\downarrow}, \delta j_{d\downarrow}^\mp d_\uparrow^\dagger\} \rangle$ in Eq. (B12) vanishes due to the orthogonality condition of basis operators, and the third term also vanishes by using Eq. (B4), where all the commutators and anticommutators vanish. In contrast, the second term must be rigorously calculated because it is non-vanishing. Using Eq. (B4), the second term is written as

$$\begin{aligned} & \langle \{d_\uparrow \delta n_{d\downarrow}, \delta j_{d\downarrow}^\mp d_\uparrow^\dagger\} \rangle = \langle d_\uparrow d_\uparrow^\dagger [n_{d\downarrow}, j_{d\downarrow}^\mp] \rangle + \langle \delta j_{d\downarrow}^\mp \delta n_{d\downarrow} \rangle \\ & = \langle (1 - n_{d\uparrow}) [n_{d\downarrow}, j_{d\downarrow}^\mp] + \delta j_{d\downarrow}^\mp \delta n_{d\downarrow} \rangle \\ & = \langle (\frac{1}{2} - n_{d\uparrow}) [n_{d\downarrow}, j_{d\downarrow}^\mp] + \frac{1}{2} [\delta n_{d\downarrow}, \delta j_{d\downarrow}^\mp] + \delta j_{d\downarrow}^\mp \delta n_{d\downarrow} \rangle \\ & = \frac{1}{2} \langle (1 - 2n_{d\uparrow}) [n_{d\downarrow}, j_{d\downarrow}^\mp] + \{\delta n_{d\downarrow}, \delta j_{d\downarrow}^\mp\} \rangle \\ & = \frac{1}{2} \langle \{ (1 - 2n_{d\uparrow}) [n_{d\downarrow}, j_{d\downarrow}^\mp] + (1 - 2\langle n_{d\downarrow} \rangle) \langle j_{d\downarrow}^\mp \rangle \} \rangle. \end{aligned}$$

Thus, the matrix elements of $i\mathbf{C}_{\mathbf{k}j\mp}$ in the block $i\mathbf{L}_{dL}$ for the SRAIM are written as:

$$\begin{aligned} i\mathbf{C}_{\mathbf{k}j\mp} &= -\langle\{i\mathbf{L}(c_{k\uparrow}^L\delta n_{d\downarrow}), \delta j_{d\downarrow}^{\mp} d_{\uparrow}^{\dagger}\}\rangle \\ &= \frac{\tilde{V}^L \langle i(1-2n_{d\uparrow})[n_{d\downarrow}, j_{d\downarrow}^{\mp}] \rangle + i(1-2\langle n_{d\downarrow} \rangle) \langle j_{d\downarrow}^{\mp} \rangle}{2 \langle (\delta n_{d\downarrow})^2 \rangle^{1/2} \langle (\delta j_{d\downarrow}^{\mp})^2 \rangle^{1/2}} \\ &\equiv \tilde{V}^L \xi_{\mp 1}, \end{aligned} \quad (\text{B13})$$

where the second term of the numerator is the imaginary part of $\tilde{V}^L \xi_{\mp 1}$, which vanishes at half-filling, as is the case in this study. Here, we explicitly include the reservoir index L to indicate that \tilde{V}^L originates from the operator $c_{k\uparrow}^L$, rather than $j_{d\downarrow}^{\mp}$. Notably, the third term in Eq. (B12), $-\langle\{c_{k\uparrow} j_{d\downarrow}^{\mp}, \delta j_{d\downarrow}^{\mp} d_{\uparrow}^{\dagger}\}\rangle$, becomes

$-\langle\{c_{k\uparrow}^L(j_{d\downarrow}^{-L} + j_{d\downarrow}^{-R}), \delta j_{d\downarrow}^{\mp} d_{\uparrow}^{\dagger}\}\rangle$ for the TRAIM. The second part, $-\langle\{c_{k\uparrow}^L j_{d\downarrow}^{-R}, \delta j_{d\downarrow}^{\mp} d_{\uparrow}^{\dagger}\}\rangle$, reflecting the left-right entanglement, is nonvanishing and expressed as $\tilde{V}^{\nu} \xi_{\mp 2}^{\nu\nu'}$, where the reservoir index of \tilde{V}^{ν} follows that of $c_{k\uparrow}$. Consequently, for the TRAIM, we write:

$$i\mathbf{C}_{\mathbf{k}j\mp}^{\nu\nu'} \equiv \tilde{V}^{\nu} \xi_{\mp 2}^{\nu\nu'}, \quad (\text{B14})$$

where $\tilde{V}^{\nu} \xi_{\mp 2}^{\nu\nu'} = \tilde{V}^{\nu} (\xi_{\mp 1}^{\nu\nu'} + \xi_{\mp 2}^{\nu\nu'})$. We factorized \tilde{V}^{ν} for use in forming the self-energy, $\Sigma_0^{\nu}(\omega) = \Sigma_{\mathbf{k}}(\tilde{V}^{\nu})^2/(\omega - \epsilon_{\mathbf{k}})$. The first term, $\tilde{V}^{\nu} \xi_{\mp 1}^{\nu\nu'}$, is given in Eq. (B13), and the second term, $\tilde{V}^{\nu} \xi_{\mp 2}^{\nu\nu'}$, is written as:

$$\tilde{V}^L \xi_{-2}^{LL} = \frac{2\langle\{c_{k\uparrow}^L(j_{d\downarrow}^{-L} + j_{d\downarrow}^{-R}), \delta j_{d\downarrow}^{-L} d_{\uparrow}^{\dagger}\}\rangle^{\text{sn}}}{\langle(\delta j_{d\downarrow}^{-L})^2\rangle^{1/2}} = \frac{2\langle c_{k\uparrow}^L d_{\uparrow}^{\dagger} [j_{d\downarrow}^{-R}, j_{d\downarrow}^{-L}] \rangle^{\text{sn}}}{\langle(\delta j_{d\downarrow}^{-L})^2\rangle^{1/2}} \text{ from } i\mathbf{C}_{\mathbf{k}j}^{LL}, \quad (\text{B15})$$

$$\tilde{V}^L \xi_{-2}^{LR} = \frac{2\langle\{c_{k\uparrow}^L(j_{d\downarrow}^{-L} + j_{d\downarrow}^{-R}), \delta j_{d\downarrow}^{-R} d_{\uparrow}^{\dagger}\}\rangle^{\text{sn}}}{\langle(\delta j_{d\downarrow}^{-L})^2\rangle^{1/2}} = \frac{2\langle c_{k\uparrow}^L d_{\uparrow}^{\dagger} [j_{d\downarrow}^{-L}, j_{d\downarrow}^{-R}] \rangle^{\text{sn}}}{\langle(\delta j_{d\downarrow}^{-R})^2\rangle^{1/2}} \text{ from } i\mathbf{C}_{\mathbf{k}j}^{LR}, \quad (\text{B16})$$

$$\tilde{V}^L \xi_{+2}^{LL} = \frac{2\langle\{c_{k\uparrow}^L(j_{d\downarrow}^{-L} + j_{d\downarrow}^{-R}), \delta j_{d\downarrow}^{+L} d_{\uparrow}^{\dagger}\}\rangle^{\text{sn}}}{\langle(\delta j_{d\downarrow}^{+L})^2\rangle^{1/2}} = \frac{2\langle c_{k\uparrow}^L d_{\uparrow}^{\dagger} [j_{d\downarrow}^{-L}, j_{d\downarrow}^{+L}] \rangle^{\text{sn}}}{\langle(\delta j_{d\downarrow}^{+L})^2\rangle^{1/2}} + \frac{2\langle c_{k\uparrow}^L d_{\uparrow}^{\dagger} [j_{d\downarrow}^{-R}, j_{d\downarrow}^{+L}] \rangle^{\text{sn}}}{\langle(\delta j_{d\downarrow}^{+L})^2\rangle^{1/2}} \text{ from } i\mathbf{C}_{\mathbf{k}j}^{LL}, \quad (\text{B17})$$

$$\tilde{V}^L \xi_{+2}^{LR} = \frac{2\langle\{c_{k\uparrow}^L(j_{d\downarrow}^{-L} + j_{d\downarrow}^{-R}), \delta j_{d\downarrow}^{+R} d_{\uparrow}^{\dagger}\}\rangle^{\text{sn}}}{\langle(\delta j_{d\downarrow}^{+L})^2\rangle^{1/2}} = \frac{2\langle c_{k\uparrow}^L d_{\uparrow}^{\dagger} [j_{d\downarrow}^{-R}, j_{d\downarrow}^{+R}] \rangle^{\text{sn}}}{\langle(\delta j_{d\downarrow}^{+R})^2\rangle^{1/2}} + \frac{2\langle c_{k\uparrow}^L d_{\uparrow}^{\dagger} [j_{d\downarrow}^{-L}, j_{d\downarrow}^{+R}] \rangle^{\text{sn}}}{\langle(\delta j_{d\downarrow}^{+R})^2\rangle^{1/2}} \text{ from } i\mathbf{C}_{\mathbf{k}j}^{LR}. \quad (\text{B18})$$

Note that $\tilde{V}^{\nu} \xi_{\mp 2}^{\nu\nu'}$ are the quantities obtained at steady-state nonequilibrium. Therefore, we denote the superscript 'sn'. The dynamics occurring in $\tilde{V}^{\nu} \xi_{\mp 2}^{\nu\nu'}$ are substantially the same as those of the γ 's in Eq. (B9), whose entangled-state tunneling dynamics are illustrated in Fig. 5 of the main text. Meanwhile, the above expressions yield the inequality:

$$|\xi_{-2}^{LL}| = |\xi_{-2}^{LR}| < |\xi_{+2}^{LL}| = |\xi_{+2}^{LR}|, \quad (\text{B19})$$

which is used in determining the inequalities among the self-energy coefficients, η_{pq} , below.

Appendix C: Self-energy coefficients η_{pq} .

The matrix reduction technique explained in Appendix A yields the equation for the Laplace-transformed on-site Green's function as:

$$(\mathbf{M}_{dd} - \mathbf{M}_{Ld} \mathbf{M}_{LL}^{-1} \mathbf{M}_{dL} - \mathbf{M}_{Rd} \mathbf{M}_{RR}^{-1} \mathbf{M}_{dR}) \mathbf{C}^d = \mathbf{I}_5, \quad (\text{C1})$$

where $\mathbf{C}^d = (A_2(z), A_1(z), i\mathcal{G}_{dd\uparrow}^+(z), A_{-1}(z), A_{-2}(z))^T$ and $\mathbf{I}_5 = (00100)^T$. Some elements of the matrix \mathbf{M} were shown in Eq. (B14) with Eqs. (B11) and (B15) – (B18), and other elements are depicted in Fig. 6. Thus, the latter two terms in the parentheses of Eq. (C1), i.e., $-\mathbf{M}_{Ld} \mathbf{M}_{LL}^{-1} \mathbf{M}_{dL} - \mathbf{M}_{Rd} \mathbf{M}_{RR}^{-1} \mathbf{M}_{dR}$, result in a 5×5 matrix with elements $i\Sigma_{pq} = \eta_{pq} [i\Sigma_0^L(\omega) + i\Sigma_0^R(\omega)]$, where $i\Sigma_0^{\nu}(\omega) = i(\tilde{V}^{\nu})^2 \Sigma_{\mathbf{k}} [1/(\omega - \epsilon_{\mathbf{k}})]$, indicating the self-energy of the non-interacting Anderson model. The matrix calculation of $-\mathbf{M}_{Ld} \mathbf{M}_{LL}^{-1} \mathbf{M}_{dL}$ yields the coefficients η_{pq} as follows:

$$\begin{aligned} \eta_{11} &= |\xi_{-}^{LL}|^2, & \eta_{12} &= \xi_{-}^{LL*} \xi_{+}^{LL}, & \eta_{14} &= \xi_{-}^{LL*} \xi_{+}^{LR}, \\ \eta_{15} &= \xi_{-}^{LL*} \xi_{-}^{LR}, & \eta_{22} &= |\xi_{+}^{LL}|^2, & \eta_{24} &= \xi_{+}^{LL*} \xi_{+}^{LR}, \\ \eta_{25} &= \xi_{+}^{LL*} \xi_{-}^{LR}, & \eta_{44} &= |\xi_{+}^{LR}|^2, & \eta_{45} &= \xi_{+}^{LR*} \xi_{-}^{LR}, \\ \eta_{55} &= |\xi_{-}^{LR}|^2, & \eta_{33} &= 1. \end{aligned}$$

with $\eta_{qp} = \eta_{pq}^*$ for $p \neq q$, while $-\mathbf{M}_{Rd} \mathbf{M}_{RR}^{-1} \mathbf{M}_{dR}$ gives the same η_{pq} with L and R exchanged. Half-filling, as in this study, gives rise to real $\xi_{\mp 2}^{\nu\nu'}$, resulting in real and

positive η_{pq} .

We now discuss the standard value, $\eta_{pq} = 1/4$, used for the phenomenological determination of η_{pq} in the main text. In item (d) of the atomic limit analysis presented in the main text, we mentioned that our differential conductance formula, Eq. (3) in the main text, yields Coulomb peaks at $\pm U/2$ at the atomic limit when the matrix elements $U_{j\mp}^{\nu'}$ are $U/4$, along with $\gamma^{L,R} = \gamma_{S,A}^{LR} = 0$.

The rationale behind this statement lies in the relationship obtained by comparing the expressions of $U_{j\mp}^{\nu'}$ in Eq. (B6) and $\xi_{\mp 1}$ in Eq. (B13):

$$\begin{aligned} \xi_{\mp 1}^{\nu\nu'} &= \frac{\langle i(1 - 2n_{d\uparrow})[n_{d\downarrow}, j_{d\downarrow}^{\mp\nu'}] \rangle + i(1 - 2\langle n_{d\downarrow} \rangle) \langle j_{d\downarrow}^{\mp\nu'} \rangle}{\langle (\delta j_{d\downarrow}^{\mp\nu'})^2 \rangle^{1/2}} \\ &= 2U_{j\mp}^{\nu'}/U, \end{aligned} \quad (\text{C2})$$

where we applied $\langle (\delta n_{d\downarrow})^2 \rangle^{1/2} = 1/2$, valid for half-filling, to the denominator of Eq. (B13). Consequently, one can see that $U_{j\mp}^{\nu'} = U/4$ amounts to $\xi_{\mp 1}^{\nu\nu'} = 1/2$, which represents the non-entangled portion of $\xi_{\mp 1}^{\nu\nu'}$. The above expressions of η_{pq} , derived from the multiplications of $\xi_{\mp 1}^{\nu\nu'}$, thus result in $(1/2)^2$, representing the non-entanglement contribution. Therefore, we arrive at the standard value, $\eta_{pq} = 1/4$.

Meanwhile, the contributions from the left-right entanglement are given by $\xi_{\mp 2}^{\nu\nu'}$, which have the inequality relationship given in Eq. (B19), which naturally leads to the η_{pq} inequalities, such as: $\eta_{11} = \eta_{15} = \eta_{55} < \eta_{12} = \eta_{14} = \eta_{25} = \eta_{45} < \eta_{22} = \eta_{24} = \eta_{44}$. We used this relationship to phenomenologically determine the values of η_{pq} used in the main text.

-
- [1] D. Goldhaber-Gordon *et al.* Phys. Rev. Lett. **81**, 5225 (1998).
 - [2] D. Goldhaber-Gordon *et al.* Nature **391**, 156 (1998).
 - [3] S. M. Cronenwett *et al.* Phys. Rev. Lett. **88**, 226805 (2002).
 - [4] S. Sarkozy *et al.* Phys. Rev. B **79**, 161307(R) (2009).
 - [5] Y. Ren, W. W. Yu, S. M. Frolov, and J. A. Folk, Phys. Rev. B **82**, 045313 (2010).
 - [6] T. Rejec and Y. Meir, Nature **442**, 900 (2006).
 - [7] K.-F. Berggren and I. I. Yakimenko, J. Phys.: Condens. Matter **20**, 164203 (2008).
 - [8] Y. Meir and N. S. Wingreen, Phys. Rev. Lett. **68**, 2512 (1992).
 - [9] J. Hong, J. Phys.: Condens. Matter **23**, 225601 (2011).
 - [10] J. Hong, J. Phys: Condens. Matter. **23**, 275602 (2011).
 - [11] P. Fulde, *Electronic Correlations in Molecules and Solids* (Springer-Verlag, Berlin, 1993) p. 116.
 - [12] J. Hong and W. Woo, Phys. Rev. Lett. **99**, 196801 (2007).
 - [13] P. O. Löwdin, J. Math. Phys. **3**, 969 (1962).
 - [14] V. Mujica, M. Kemp, and M. A. Ratner, J. Chem. Phys. **101**, 6849 (1994).
 - [15] A. C. Hewson, *The Kondo Problem to Heavy Fermions* (Cambridge University Press, Cambridge, 1993) p. 13.
 - [16] J. Hong and D. S. L. Abergel, Sci. Rept. **6**, 31352 (2016).
 - [17] J. Hong, J. Phys: Condens. Matter **31**, 375602 (2019).